Order−Disorder and Direct Evidence of Oxygen Vacancies in a New Family of BICUWOX Compounds

David Ávila-Brande,[†] Ángel R. Landa-Cánovas,[‡] and L. Carlos Otero-Díaz*[,†,§]

Departamento Química Inorgánica, Facultad CC. Químicas, Universidad Complutense, E-28040 Madrid, Spain, Instituto de Ciencia de Materiales de Madrid, CSIC, E-28049 Madrid, Spain, and Centro de Microscopía, Universidad Complutense, E-28040 Madrid, Spain

Received September 21, 2006. Revised Manuscript Received November 3, 2006

During the synthesis of the compound with nominal composition $Bi_4Cu_{1/3}W_{2/3}O_{7.8}Cl$, a new family of compounds, which can be described as ordered intergrowth of one Sillén block $[Bi_2O_2Cl]$ and *n* oxygen deficient blocks $[Bi_2Cu_{1/(2n+1)}W_{2n/(2n+1)}O_{6-\delta}]_n$ with $\delta = 0.18$, was produced. Transmission electron microscopy and associated techniques were used to determine the composition, unit-cell symmetry, and space group of the main phase corresponding to the $n = 1$ member $Bi_4Cu_{1/3}W_{2/3}O_{8-\delta}Cl$. Structural models for both compounds $n = 1$ and $n = 2$ were deduced by exit wave reconstruction in a crystal where these phases were intergrown. The existence of the highest members $n = 3$ and 4 was confirmed by HREM in several crystallites, in which we have found the compounds with $n = 1-4$ as disordered intergrowths. Moreover, some crystals with cationic ordering in the octahedral layer were also found. Oxygen atoms and vacancies were imaged using the exit wave reconstruction technique in the structure determination of the first Sillén-BICUWOX intergrowth. The average structure of the main phase $Bi_4Cu_{1/3}W_{2/3}O_{8-\delta}Cl$ was refined from X-ray powder diffraction data using the Rietveld method, yielding a tetragonal unit cell with lattice parameters $a = 3.845(9)$ Å, $c = 14.188(7)$ Å (space group *P*4/*mmm* No. 123), which could be described as a Sillén−Aurivillius oxygen deficient intergrowth.

Introduction

The layered bismuth oxides with general formula $Bi_2A_{n-1}B_nO_{3n+3}$ were first described by Aurivillius[1] and are structurally related to Ruddlesden−Popper[2] and Dion−Jacobsen[3] phases. Their structure is composed of $[Bi_2O_2]^{2+}$ sheets in which the oxygens form the basal square plane of chessboard-like pattern square pyramids, with Bi in the apex pointing above and below the layer, interleaved with perovskite layers $[A_{n-1}B_nO_{3n+3}]^{2-}$ (*n* denotes the octahedral thickness). Up to now, compounds with $n = 1-5$ have been synthesized, e.g., Bi_2WO_6, $Bi_4Ti_3O_{12}$....[4−6] These layered two-dimensional perovskites have attracted much attention because of their interesting ferroelectric properties with high Curie temperatures in the development of technological applications such as FRAM devices.[7] Besides, the new phases of Bi-based high-temperature superconductors closely related to Aurivillius family[8] enhanced the research devoted to finding new superconductors structurally related to these phases.

The oxygen-deficient compounds with Aurvillius related structures have led to intense research after the ion-conducting properties were determined for the $Bi_4V_2O_{11}$ phase.[9] This compound presents three phase transitions $\alpha \rightarrow \beta \rightarrow \gamma$, with the γ polymorph showing the largest ionic conductivity.[10] In this sense, many synthetic efforts have been carried out that are mainly devoted to stabilizing the γ-phase by isomorphic substitution of V or Bi. As result, many different compounds generally called BIMEVOX ($Bi_4V_{1-x}M_xO_{11-\delta}$, M = Cu^{2+}, Ni^{2+}, Fe^{3+}, Mn^{3+}...) have been characterized, and their ionic conductivity properties have been analyzed.[11−13]

The bismuth oxyhalides, prepared by Sillén, consist of alternating $[Bi_2O_2]^{2+}$ sheets, described above, and *m* (1, 2, or rarely 3) halogen layers.[14]

Because of the similarities in structure (the presence of the $[Bi_2O_2]^{2+}$ unit), the intergrowth of Aurivillius and Sillén phases can be easily envisaged.[15] The general formula of this intergrowth can be written as $[Bi_2O_2][A_{n-1}B_nO_{3n+1}][Bi_2O_2][X_m]$, where *n* denotes the thickness of the perovskite layers in terms of BO_6 octahedra and *m* the number of halogen (X =

* Corresponding author. E-mail: carlos1@quim.ucm.es.
† Departamento Química Inorgánica, Universidad Complutense.
‡ CSIC.
§ Centro de Microscopía, Universidad Complutense.

(1) *Structural Inorganic Chemistry*; Wells, A. F., Ed.; Clarendon Press: Oxford, U.K., 1975.
(2) Ruddlesden, S. N.; Popper, P. *Acta Crystallogr.* **1958**, *11*, 54.
(3) (a) Dion, M.; Ganne, M.; Tournoux, M. *Mater. Res. Bull.* **1981**, 16, 1429. (b) Jacobson, A. J.; Johnson, J. W.; Lewandowski, J. T. *Inorg. Chem.* **1985**, 24, 3727.
(4) Aurivillius, B. *Ark. Kemi* **1950**, *1*, 463.
(5) Aurivillius, B. *Ark. Kemi* **1950**, *2*, 519.
(6) Aurivillius, B. *Ark. Kemi* **1952**, *5*, 39.
(7) Scott, J. F. *Phys. World* Feb. 1995, 47.
(8) Withers, R. L.; Thompson, J. G.; Wallenberg, L. R.; Fitzgerald, J. D.; Anderson, J. S.; Hyde, B. G. *J. Phys. C: Solid State Phys.* **1988**, *21*, 6067.
(9) Buch, A. A.; Venetsev, Y. N. *Russ. J. Inorg. Chem.* **1986**, *31*, 769.
(10) Vannier, R. N.; Pernot, E.; Anne, M.; Isnard, O.; Nowogrocki, G.; Mairesse, G. *Solid State Ionics* **2003**, *157*, 147.
(11) Lee, C. K.; Lim, G. S.; West, A. R. *J. Mater. Chem.* **1994**, *4*, 1441.
(12) Yan, J.; Greenblatt, M. *Solid State Ionics* **1995**, *81*, 255.
(13) Joubert, O.; Ganne, M.; Vannier, R. N.; Mairesse, G. *Solid State Ionics* **1996**, *83*, 199.
(14) Sillén, L. G. X-ray studies on oxides and oxyhalides of trivalent bismuth. Inaugural dissertation, Stockholm, Sweden, 1940.
(15) Aurivillius, B. *Chem. Scr.* **1980**, *5*, 153.

10.1021/cm062263j CCC: $37.00
Published on Web 12/15/2006

Cl, Br) slabs. To date, several compounds within this family have been synthesized, e.g., Bi_4MO_8X ($M = Nb^{5+}$, Ta^{5+} and $X = Cl$, Br),[16−18] $Bi_5PbTi_3O_{14}Cl$.[19] The ideal space group of those compounds is *P*4/*mmm*, although refinements carried out mainly by means of neutron diffraction have shown lower symmetries, leading to orthorhombic space groups. On the other hand, the study of the symmetry, the local structure, and the presence of defects using transmission electron microscopy and associated techniques has been performed recently over the series of compounds $Bi_4M'_xM_{1-x}O_8X$ ($M = W^{6+}$; $M' = Ti^{4+}$, Mn^{3+}; $X = Cl$, Br).[20,21]

If these results are taken into account, the intergrowth between the Sillén and the oxygen deficient compounds (BIMEVOX) could be possible and a large number of compounds with interesting properties could be synthesized.

This work deals with the synthesis, structure determination, and microstructural characterization of the first Sillén−BICUWOX intergrowth with nominal composition $Bi_4Cu_{1/3}W_{2/3}O_{7.8}Cl$.

Experimental Section

Preparation of the Samples. A polycrystalline sample with nominal composition $Bi_4Cu_{1/3}W_{2/3}O_{7.8}Cl$, has been prepared by heating the stoichiometric amounts of the oxides Bi_2O_3 (4N), WO_3 (4N), CuO (4N), and BiOCl (4N) at 993 K in air for 48 h and quenching to room temperature.

Characterization of the Samples. Samples for TEM were prepared by ultrasonic dispersion of the powder in *n*-butanol. Drops of this dispersion were deposited on a holey carbon-coated copper grid. A JEOL 2000FX equipped with a LINK ISIS 300 analyzer has been used for XEDS analysis, microdiffraction, and SAED. EELS spectra were acquired using a Philips CM200 FEG TEM equipped with a Gatan image filter (GIF) 200 with 0.95 eV energy resolution. HRTEM was performed using a JEOL 3000F TEM, yielding an information limit of 1.1 Å. The exit wave has been reconstructed from the focal series using the IWFR software.[22] HRTEM images simulations were performed with the WinHREM software.[23]

X-ray powder diffraction patterns were recorded on a Siemens D-501 ($CuK_{\alpha 1}$ radiation $\lambda = 1.5406$ Å) over the angular range 10−100°, with a step scan of 0.04°. Rietveld full-profile refinement was done with the FULLPROF program.[24] A pseudo-Voigt function was chosen to generate the line shape of the diffraction peaks. In the final runs, the following parameters were refined: scale factor, background point to point, unit-cell parameters, asymmetry parameters, positional coordinates, and isotropic thermal parameters. Because of the stronger X-ray scattering of Bi^{3+}, Cu^{2+}, and W^{6+}, the isotropic atomic displacement parameters (ADPs) of chlorine and oxygen atoms were all fixed at a reasonable value of 0.8 Å.[2] Because of the oxygen vacancies, the ADPs of W^{6+} and Cu^{2+} were not refined and were fixed at a value of 0.5 Å.[2]

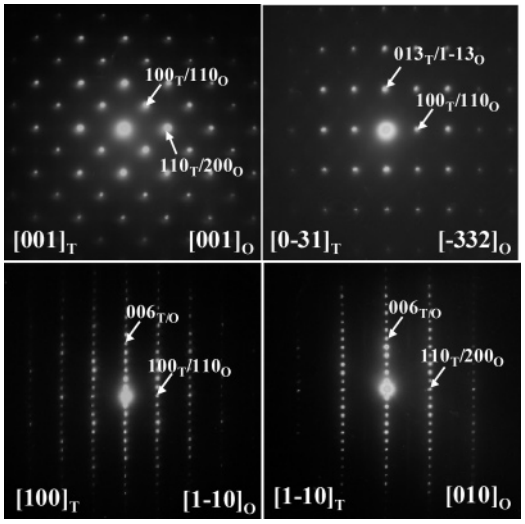

Figure 1. SAED patterns along the zone axes $[001]_T/[001]_O$, $[0\bar{3}1]_T/[\bar{3}32]_O$, $[100]_T/[1\bar{1}0]_O$ and $[1\bar{1}0]_T/[010]_O$ of the $Bi_4Cu_{1/3}W_{2/3}O_{8-\delta}Cl$ crystals.

EPR measurements were carried out at 77 K with a Bruker ER200D spectrometer provided with a T-type double cavity and operating in the X-band (9.55 GHz). Frequency calibration was performed using a 2,2-diphenyl-1-picrylhydrazine (DPPH) standard ($g = 2.0036$). All of the spectra were recorded at 77 K using a microwave power of 19 mW.

Magnetic susceptibility measurements were performed on polycrystalline sample between 2 and 300 K, using a Quantum Design SQUID MPMS-X.

Results and Discussion

The SAED (selected area electron diffraction) study of the reciprocal space shows that the reflection conditions are consistent either with a primitive P tetragonal unit cell ($a_o = b_o = 3.8$ Å and $c_o = 14.1$ Å) or a pseudotetragonal one ($a \approx b = \sqrt{2}a_o = 5.4$ Å and $c = 14.1$ Å) with *C* centering (*hkl*, $h + k = 2n$). (Figure 1).

The semiquantitative XEDS (X-ray energy dispersive spectroscopy) analysis of the composition over 10 crystals yields an average composition of $Bi_{3.98(4)}Cu_{0.30(3)}W_{0.69(6)}Cl_{1.03(4)}$, close to the nominal composition. However, because of the overlapping between the $Bi-M_\alpha$ and the $Cl-K_\alpha$ peaks, the presence of Cl cannot be asserted and some EELS (electron energy loss spectroscopy) experiments were performed, where the broad $L_{2,3}$ absorption edge at 200 eV proves the presence of the chlorine in the structure (Figure 2).

Choosing between a primitive cell (*a*, *b*, *c*) and a *C*-centered one with $a = \sqrt{2}a_o$, $b = \sqrt{2}a_o$, and *c* unit-cell parameters is actually just a convention, because both cells are equivalent. SAED would never distinguish between both cases, because the same reflections would be present with the same spacings changing only the nomenclature of the *hkl* indices, e.g., the 110 primitive cell reflection would be equivalent to the 200 centered cell reflection.

The point group of a crystal system can be determined by observing the "ideal" symmetries of CBED (convergent beam electron diffraction) zone axes patterns.[25,26] The zero-order

(16) Ackerman, J. F. *J. Solid State Chem.* **1986**, *62*, 92.
(17) Kusainova, A. M.; Stefanovich, S. Y.; Dolgikh, V. A.; Mosunov, A. V.; Hervoches, C. H.; Lightfoot P. *J. Mater. Chem.* **2001**, *11*, 1141.
(18) Kusainova, A. M.; Zhou, W.; Irvine, J. T. S.; Lightfoot, P. *J. Solid State Chem.* **2002**, *166*, 148.
(19) Kusainova, A. M.; Stefanovich, S. Y.; Irvine, J. T. S.; Lightfoot, P. *J. Mater. Chem.* **2002**, *12*, 3413.
(20) Ávila-Brande, D.; Gómez-Herrero, A.; Landa-Cánovas, A. R.; Otero-Díaz, L. C. *Solid State Sci.* **2005**, *7*, 486.
(21) Ávila-Brande; D.; Landa-Cánovas, A. R.; Otero-Díaz, L. C.; Bals, S.; Van Tendeloo, G. *Eur. J. Inorg. Chem.* **2006**, *9*, 1853.
(22) *IWFR*, version 1.0; HREM Research Inc.: Higashimastuyama, Japan, Feb 2005.
(23) *Win-HREM*, version 2.5; HREM Research Inc.: Higashimastuyama, Japan, 1998.
(24) Rodriguez Carvajal, J. *Fullprof.2k*, version 1.9c; Laboratoire Léon Brillouin: Gif-sur-Yvette, France, May 2001.

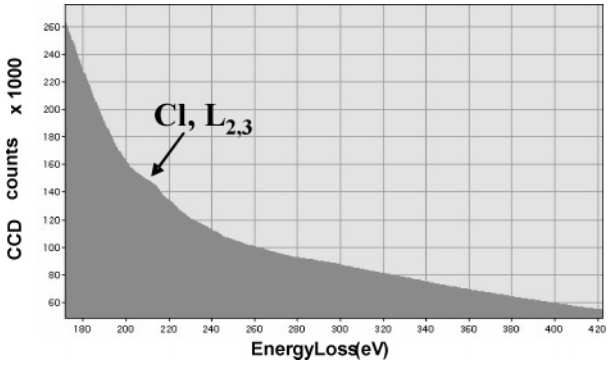

Figure 2. EELS spectrum showing the chlorine $L_{2,3}$ absorption edge at 200 eV.

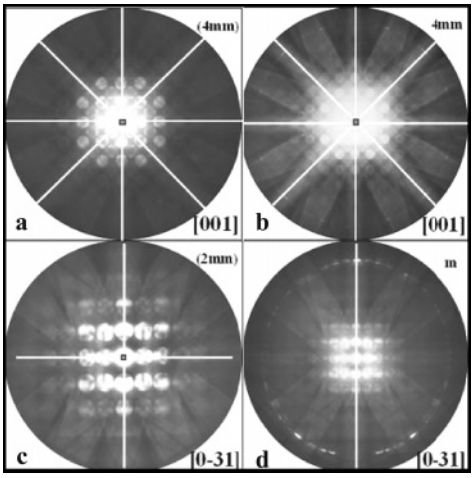

Figure 3. (a) BF (bright field) and (b) WP (whole pattern) CBED patterns taken along the [001] zone axis. (c) BF and (d) WP CBED patterns taken along the [0$\bar{3}$1] zone axis.

Laue zone (ZOLZ) ideal symmetry of the [001] zone axis pattern (Figure 3a) is 4*mm*, indicating that the crystal system must present tetragonal symmetry; the whole pattern (WP) ideal symmetry (Figure 3b) is also 4*mm*. The observed symmetries along [001] are in agreement with the 4/*mmm* and 4*mm* point groups. In order to distinguish between them a CBED pattern was taken along [0$\bar{3}$1]. Figure 3c shows the ideal ZOLZ symmetry to be 2*mm*, whereas the ideal WP symmetry observed in Figure 1d is *m*. The ideal symmetry is in agreement only with the point group 4/*mmm* (see the Supporting Information). A primitive tetragonal unit cell presenting the point group 4/*mmm* without any systematic extinction allows us to choose the *P*4/*mmm* space group.[27]

Although HRTEM (high-resolution transmission electron microscopy) shows in most of the crystals a well-ordered structure, it is remarkable that in some interesting cases, it reveals the presence of defects (see Figure 4). The contrast on the right corresponds to a well-ordered crystal with an average period of 14.1 Å along *c* (marked with white arrows), which is composed of the periodic simple intergrowth of one Sillén layer [Bi_2O_2Cl] with one oxygen deficient Aurivillius block [$Bi_2W/CuO_{6-\delta}$]. Otherwise, on the left part of the image,

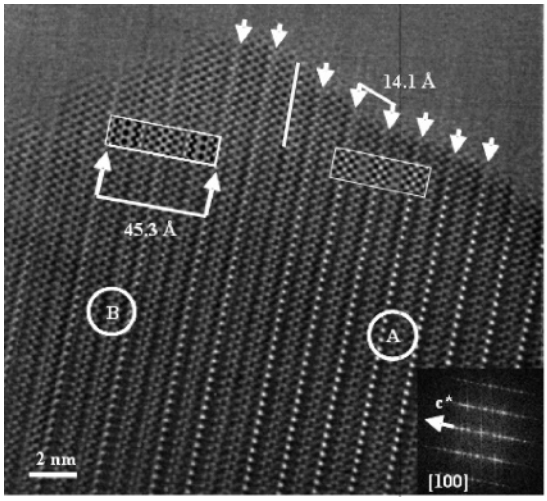

Figure 4. HRTEM image along [100] where the basic structure (area marked by A) intergrows with the superstructure with $c = 45.3$ Å (area marked by B). The simulated images from the models determined after exit wave reconstruction at defocus value of $\Delta f = -200$ Å and a thickness $t = 80$ Å are shown as inset. Notice the stacking fault marked with a white line.

we can see extended defects locally ordered in the matrix of the majority phase yielding a new superstructure with $c = 45.3$ Å. Those defects are responsible for the streaking observed along *c** in the fast Fourier transform (FFT) pattern.

To obtain information about the Cu:W ratio in these ordered defects, we performed XEDS analysis on the zones labeled as A and B in Figure 4 with a 10 nm electron probe, which can only be achieved in a FEG (field emission gun) microscope. The W:Cu ratio in the A zone, where the structure is free of defects, is 2:1 according to the nominal composition, whereas the cation ratio increases to 4:1 when the analysis probe is located in zone B, where two cells belonging to the superstructure with $c = 45.3$ Å are observed. Considering our previous HRTEM and microanalysis results, the origin of this new superstructure is the stacking faults (see one of them marked with a line in Figure 4) due to the substitution of chlorine layers $[Cl]^-$ by perovskite blocks $[W/CuO_{4-\delta}]^{3-}$, thus increasing the negative charge. Hence, to make an electroneutral compound, the positive charge must increase, reducing the amount of Cu^{2+} in favor of W^{6+}.

To obtain a complete structural model, we performed an exit wave reconstruction (EWR) experiment.[28] The goal of EWR is to achieve directly from the images a better resolution limit rather than the point resolution of the microscope. A great advantage of this technique is that the amplitude as well as the phase of the exit wave are restored. Because light atoms can be imaged in the phase of the exit wave, the phase can thus be used as starting point to determine the structural model of new compounds.[29]

We have applied EWR to determine not only the structural model of the compound $Bi_4Cu_{1/3}W_{2/3}O_{8-\delta}Cl$ but also to obtain an ideal model for the superstructure detected in the HREM image of Figure 4, where the EWR was performed. A focal series of 20 images with an equidistant focal decrease is recorded along the [100] zone axis using a slow-scan CCD

(25) Morniroli, J. P.; Steeds, J. W. *Ultramicroscopy* **1992**, *45*, 219.
(26) *Convergent-Beam Electron Diffraction*; Tanaka, M., Terauchi, M., Eds.; JEOL-Maruzen: Tokyo, 1985.
(27) *International Tables for Crystallography Vol. A*; Hahn, T., Ed.; International Union of Crystallography: Chester, U.K., 1983.
(28) Coene, W. M. J.; Thust, A.; Op de Beek, M.; Van Dyck, D. *Ultramicroscopy* **1996**, *64*, 109.
(29) Bals, S.; Van Aert, S.; Van Tendeloo, G.; Ávila Brande, D. *Phys. Rev. Lett.* **2006**, *96*, 096106.

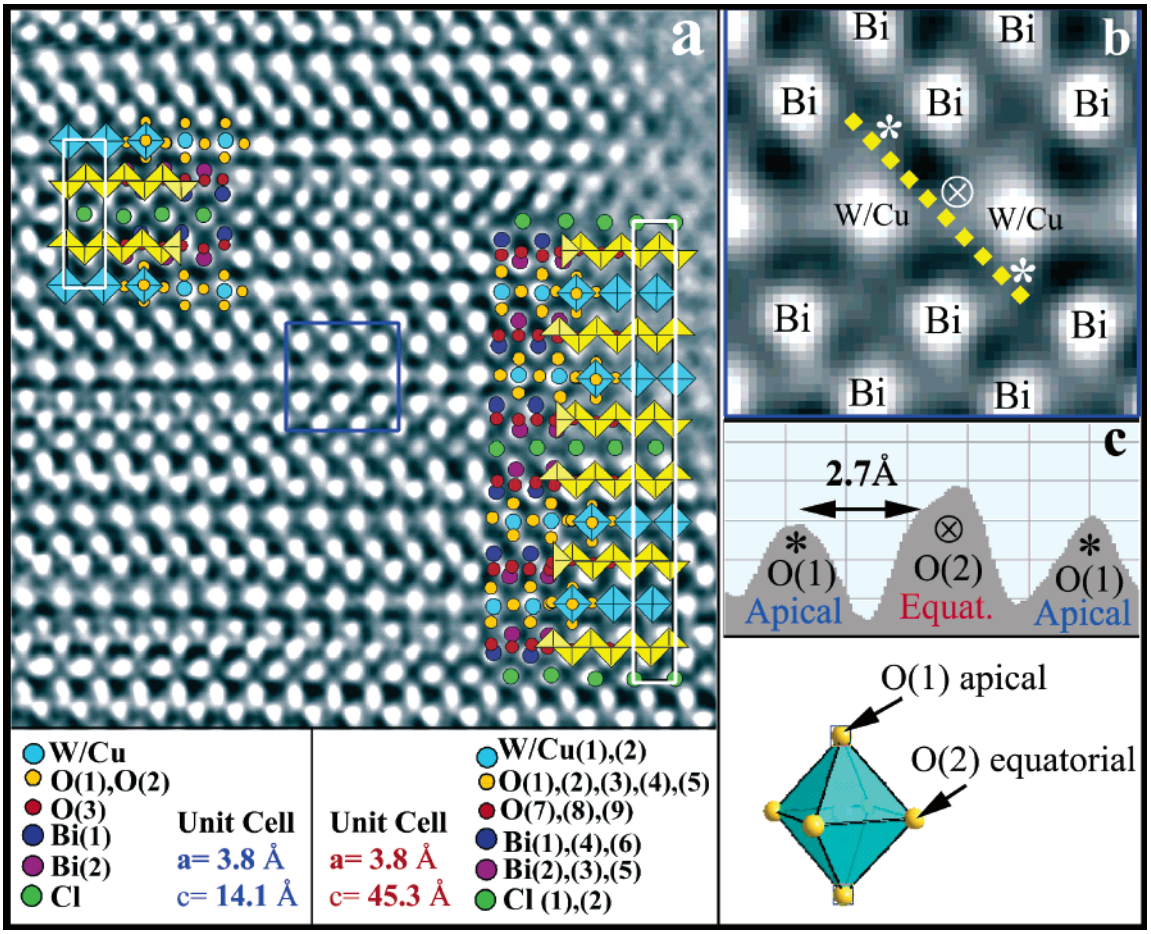

Figure 5. (a) Micrograph of the reconstructed phase obtained from a series of 20 images at different values of defocus of the same crystal displayed in Figure 4 (rotated 90°). The atomic columns for all the atoms (including oxygens) are represented by colored circles that correspond to the legends displayed in the bottom of the figure. (b) Enlargement of the squared blue section in (a) showing the perovskite layer [$W/CuO_{4-\delta}$]. Notice the fainter white dots corresponding to the oxygens surrounding the W/Cu atomic column and as elongations of the Bi dots. (c) Profile intensity variation along the line depicted in (b) from O(1) (represented by *) to O(2) (represented by ⊗) and again to O(1), indicating the location of oxygen vacancies in apical oxygens.

Table 1. Measured Coordinates from the EWR Phase Image Along [100] for the $Bi_4Cu_{1/3}W_{2/3}O_{8-\delta}Cl$ Phase

atom	Wyckoff	*x*	*y*	*z*
W/Cu	1*a*	0	0	0
Bi1	2*h*	1/2	1/2	0.21
Bi2	2*g*	0	0	0.37
Cl	1*d*	1/2	1/2	
O1	2*f*	1/2	0	0
O2	2*g*	0	0	0.10
O3	4*i*	1/2	0	0.06

camera. The reconstruction and numerical correction for the aberrations were performed using the IWFR software based in the algorithm developed by Allen et al.[30] The reconstructed phase image is presented in Figure 5a, where the overlays indicate the position of the different type of atomic columns, which appear as bright dots. It is very important to note that the light oxygen atoms are also imaged as fainter white dots.

With this direct structural information and taking into account the *P*4/*mmm* space group previously determined for $Bi_4Cu_{1/3}W_{2/3}O_{8-\delta}Cl$, we can build up its ideal structural model, overlapped in the phase image on the upper left part of the image, by measuring the projected coordinates directly in the image (see Table 1).

On the other hand, we can see in the bottom right part of the phase image the sequence of the superstructure with $a = 3.8$ Å and c-axis of 45.3 Å, which can be interpreted by the following layer stacking sequence:

$-[Cl]-[Bi_2O_2]-[W/CuO_{4-\delta}]-[Bi_2O_2]-[W/CuO_{4-\delta}]-[Bi_2O_2]-[Cl]-[Bi_2O_2]-[W/CuO_{4-\delta}]-[Bi_2O_2]-[W/CuO_{4-\delta}]-[Bi_2O_2]-$

We can simplify this long sequence with the short notation $[Bi_2O_2Cl][Bi_2W/CuO_{6-\delta}]_2$. Written in this way, it enables us to describe this defect as the intergrowth between one $m = 1$ Sillén block and two consecutive members of the $n = 1$ Aurivillius family. The projected coordinates for this ideal model can be measured from the reconstructed phase of Figure 5a (see the Supporting Information), yielding the corresponding structure model superimposed in the image. Such a kind of intergrowth has never been observed, although it was postulated by Ackerman.[16]

In this family of compounds $[Bi_2O_2Cl]_p[Bi_2W/CuO_{6-\delta}]_q$, $3p + 3q$ must be even to have a repetition unit, so for a composition $[Bi_2O_2Cl][Bi_2W/CuO_{6-\delta}]_2$, the cell content must be $[Bi_2O_2Cl]_2[Bi_2W/CuO_{6,-\delta}]_4$, in good agreement with the sequence determined from the EWR study.

In these compounds, the deficiency in oxygen could be accommodated either in the equatorial or the apical site of the perovskite layer, as was previously determined from high-

(30) Allen, L. J.; McBride, W.; Oleary, N. L.; Oxley, M. P. *Ultramicroscopy* **2004**, *100*, 91.

Table 2. New Family of Oxyhalides Determined from HRTEM Observations

n	$(Bi_2O_2Cl)(Bi_2Cu_{1/(2n+1)}W_{2n/(2n+1)}O_{6-\delta})_n$	W:Cu ratio	*c*-axis (Å)
1	$(Bi_2O_2Cl)(Bi_2Cu_{1/3}W_{2/3}O_{6-\delta})$[a]	2:1	14.1
2	$(Bi_2O_2Cl)(Bi_2Cu_{1/5}W_{4/5}O_{6-\delta})_2$[a]	4:1	45.3
3	$(Bi_2O_2Cl)(Bi_2Cu_{1/7}W_{6/7}O_{6-\delta})_3$[b]	6:1	31.2
4	$(Bi_2O_2Cl)(Bi_2Cu_{1/9}W_{8/9}O_{6-\delta})_4$[b]	8:1	78.0

[a] Experimental composition obtained from XEDS analysis in the areas marked by A and B in Figure 4. [b] Chemical composition extrapolated from the experimental ratio determined from the members $n = 1$ and 2, taking into account that the W:Cu ratio increases with the *n* value.

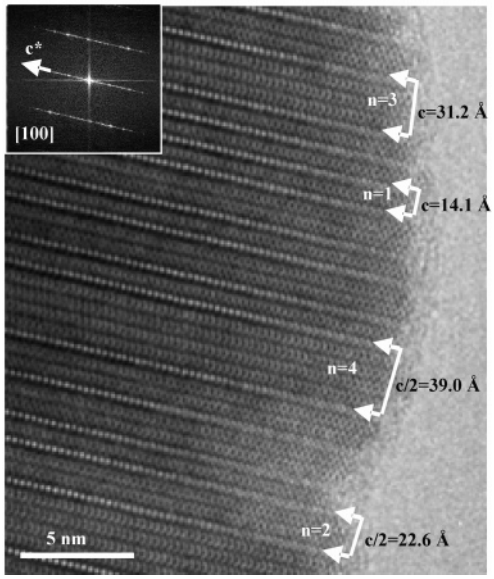

Figure 6. HRTEM image along [100] of a crystal showing the members $n = 1-4$ of the family with general composition $(Bi_2O_2Cl)(Bi_2Cu_{1/(2n+1)}W_{2n/(2n+1)}O_{6-\delta})_n$.

resolution neutron diffraction experiments in BIMEVOX compounds.[31] The enlargement of the perovskite layer from the recovered phase image (Figure 5b) provides a local direct evidence of the vacancies location. The phase of the exit wave is proportional to the projected electrostatic potential of the structure.[32] The line intensity profile along the oxygen atoms O(1) (apical site) and O(2) (equatorial), performed on this enlargement of the Aurivillius block in the phase image (Figure 5c), shows higher intensity for O(2) than O(1), so the anion vacancies should be located in the apical site O(1). The relative intensities change along the image for the different O(1)−O(2)−O(1) triads but with little variation, as shown in Figure 5b. Nevertheless, in all the cases, the vacancies in higher or lower proportion were always located in the apical oxygens O(1).

The simulated images, obtained with the two models determined from the EWR study for a defocus value $\Delta f = -200$ Å and a thickness $t = 80$ Å (Figure 4), were found to be in agreement with the experimental ones.

From these structural determinations and chemical results, we can postulate the existence of a new family of compounds formed by one Sillén block and *n* $[Bi_2W/CuO_{6-\delta}]$ blocks with general composition as displayed in Table 2. The existence of the members $n = 1-4$ is clearly evidenced by the HRTEM image of Figure 6. In this image, we can see four different

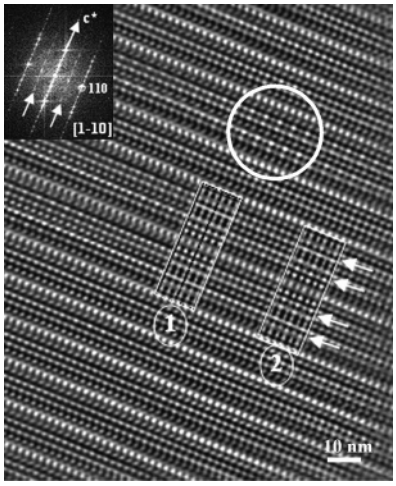

Figure 7. Filtered HRTEM image along $[1\bar{1}0]$ showing an intergrowth between phases $n = 1$ and $n = 2$. The calculated images for the $n = 2$ phase with cation disorder and cation order are labeled as 1 and 2, respectively. The white arrows show the cation arrangement along the perovskite layers.

members belonging to the family described before. In this crystal, we observe half unit cells corresponding to the members with $n = 2$ and $n = 4$, because their unit cells involve the stacking of six $[Bi_2O_2Cl]_2[Bi_2W/CuO_{6-\delta}]_4$ and ten $[Bi_2O_2Cl]_2[Bi_2W/CuO_{6-\delta}]_8$ blocks, respectively. However, the complete unit cell of the odd members composed of two $[Bi_2O_2Cl][Bi_2W/CuO_{6,-\delta}]$ or three $[Bi_2O_2Cl][Bi_2W/CuO_{6-\delta}]_2$ blocks is observed, because of their easier stacking.

Figure 7 shows the presence of disordered intergrowths between the phases $[Bi_2O_2Cl][Bi_2W/CuO_{6,-\delta}]$ and $[Bi_2O_2Cl][Bi_2W/CuO_{6,-\delta}]_2$, clearly observed and evidenced as intensity streaking along c^* in the $[1\bar{1}0]$ FFT pattern of the HRTEM image. In this pattern, we also observe weak discontinuous streak lines marked with white arrows along the *hhl:* $h = 1/2$ reflection rows. These lines indicate the presence of extra order, because they double the *hh0* reflections. In some areas of the image, marked with a white circle, this extra ordering can be observed as alternating big and small white dots. In the right part of Figure 7, two calculated images from $[Bi_2O_2Cl][Bi_2W/CuO_{6-\delta}]_2$ are displayed. The simulated image labeled 1 was calculated with Cu and W indistinctly occupying the two octahedral sites, whereas the simulated image 2 was calculated with Cu and W located in consecutive octahedra along (110), according to the projected model drawn in Figure 8. The image simulations confirm the cation ordering between Cu and W as the origin of regions with contrast variation along the perovskite layer. Moreover, the excellent fit with the experimental image enables us to validate the structural models deduced after EWR.

Once the unit cell, the space group, the structural model, and the nature of defects are determined from electron microscopy data, the refinement of the average structure of $Bi_4Cu_{1/3}W_{2/3}O_{8-\delta}Cl$ was carried out by X-ray powder diffraction (Figure 9). The Rietveld refinement was performed using the structural data obtained from the phase of the reconstructed exit wave (see Table 1). Table 3 summarizes the refined structural parameters; the *R* factors of weighted pattern (R_{wp}), pattern (R_p), Bragg (R_B), and the value of χ^2 converge to 17.4, 15.2, and 6.84% and 4.57, respectively (see the Support-

(31) Abrahams, I.; Krok, F. *J. Mater. Chem.* **2002**, *12*, 3351.
(32) Houben, L., Thust, A.; Urban K. *Ultramicroscopy* **2006**, *106*, 200.

Table 3. Refined Structural Parameters and Main Interatomic Distances for the $Bi_4Cu_{1/3}W_{2/3}O_{8-\delta}Cl$ Phase[a]

atom	site	*x*	*y*	*z*	*B* (Å^2)	bond	distance (Å)	frequency
Bi(1)	*2g*	0	0	0.367(2)	2.47(5)	Bi(1)−O(3)	2.17(8)	×4
Bi(2)	*2h*	1/2	1/2	0.187(2)	1.37(5)	Bi(2)−O(3)	2.46(9)	×4
W	*1*a	0	0	0	0.5	Bi(1)−Cl	3.30(2)	×4
Cu	*1a*	0	0	0	0.5	W/Cu−O(1)	1.72(4)	×4
Cl	*1d*	1/2	1/2		0.8	W/Cu−O(2)	1.92(3)	×2
O(1)	*2g*	0	0	0.121(6)	0.8	Bi(2)−O(1)	2.87(4)	×4
O(2)	*2f*	1/2	0	0	0.8			
O(3)	*4i*	1/2	0	0.296(1)	0.8			

[a] Space group *P/4mmm; a* = 3.846(3) Å, *c* = 14.190(1) Å; R_p= 15.2%, R_{wp}= 17.4%, R_b= 6.84%; χ^2= 4.57.

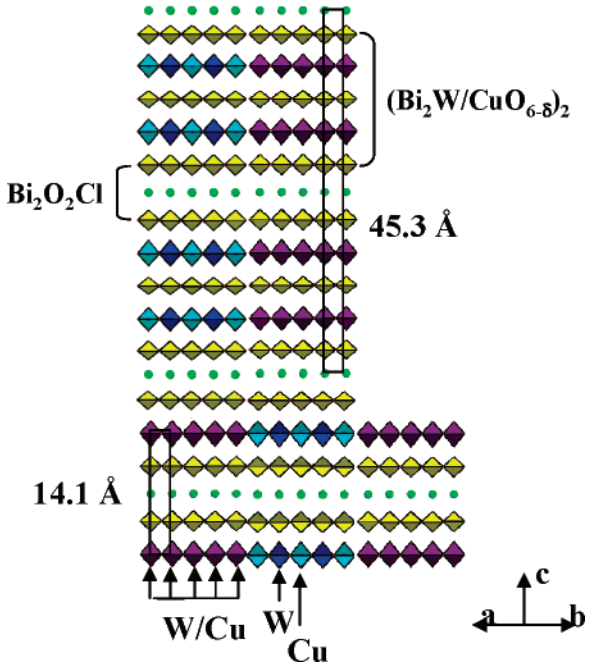

Figure 8. Schematic model of the intergrowth between the phases observed in Figure 7 showing the cation ordering. In the upper part of the drawing, the $n = 2$ member is depicted, whereas the $n = 1$ member is in the bottom. The order between W and Cu is indicated in both structures by different hues of the blue octahedra.

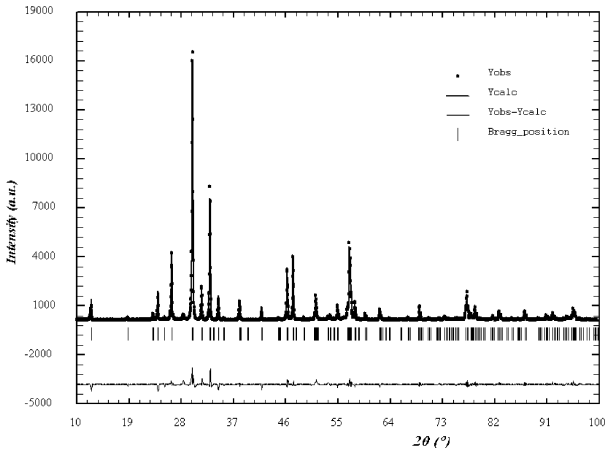

Figure 9. Experimental (circles), calculated, and difference (solid lines) powder X-ray diffraction patterns of the phase $Bi_4Cu_{1/3}W_{2/3}O_{8-\delta}Cl$. Vertical bars indicate the calculated Bragg angle positions.

ing Information). These values agree with those obtained in other Aurivillius and Sillén−Aurivillius phases.[33,34] It is worth mentioning that the high B value obtained for Bi(2) in the refinement agrees with our previous work on the related $Bi_4Ti_{1/2}W_{1/2}O_8Cl$ and $Bi_4Mn_{1/3}W_{2/3}O_8Cl$ compounds.[20,21] This high value is due to an asymmetric surrounding around the Bi_2O_2 layer, Bi(1) is close to the Cl sheet, whereas Bi(2) is much closer to the $\{BO_6\}$ octahedral layer and can establish short contacts to the apex oxygen atoms O(1) (see Table 3), changing its coordination from 4 to 5. On the other hand, the high B value of Bi(1) (see Table 3) can be explained by the presence of the defects analyzed because the substitution of one Cl sheet by a perovskite blocks $[W/CuO_{4-\delta}]^3$ induces the same effect discussed for Bi(2).

From EPR (electron paramagnetic resonance) spectra, we have calculated an effective moment of 1.82 μ_B for the Cu^{2+} in the compound. However, the magnetic susceptibility measurements (see the Supporting Information) yield a moment of 1.88 μ_B above the previous one obtained for Cu^{2+}. This difference could be due either to an spin−orbit coupling or the presence of 5% in content of paramagnetic Cu^{3+} in a high spin configuration. The fact that this phase does not synthesize in sealed quartz tubes but in open air supports the hypothesis of the partial oxidation of 5% of Cu^{2+} to Cu^{3+}, leading to an experimental composition of $Bi_4Cu_{1/3}W_{2/3}O_{8-\delta}Cl$ ($\delta = 0.18$).

Conclusions

The use of TEM, exit wave reconstruction, and electron and X-ray diffraction allow us to determine the structure of $[Bi_2O_2Cl][Bi_2Cu_{1/(2n+1)}W_{2n/(2n+1)}O_{6-\delta}]_n$, and this procedure is largely extendible to the structure determination of other unknown materials. In particular, using EWR, we were able to view the oxygen atoms which, because of their low scattering power, were not previously accessible; this allowed us to locate the position of the oxygen vacancies. Further work is needed to statistically quantify the vacancies concentration from the whole image and requires us to develop a computer routine capable of estimating the average intensity change of the oxygen maxima from the whole image and relating the intensity change to the vacancies concentration.

Acknowledgment. This work was supported by the UCM-Santander Project PR 27/05-13982. D.Á.B. is grateful to MECD for a predoctoral grant.

Supporting Information Available: Crystallographic data in CIF format; table with relations between the point group, the zone axis, and the ideal symmetry in the tetragonal system; table of measured coordinates from the ESW phase image; plot of the magnetic susceptibility vs temperature. This material is available free of charge via the Internet at http://pubs.acs.org.

CM062263J

(33) Yu, W. J.; Kim, Y. I., Ha, D. H.; Lee, J. H.; Park, Y. K., Seong, S.; Hur, N. H. *Solid State Commun.* **1999**, *111*, 705.
(34) Yang, L. Y.; Qiu, L.; Harrison, W. T. A.; Christoffersen, R.; Jacobson, A. J. *J. Mater. Chem.* **1997**, *7*, 243.